

Quantum entanglement and Einstein-Podolsky-Rosen steering in magnon frequency comb

Qianjun Zheng¹, H. Y. Yuan^{2,*}, Yunshan Cao¹, and Peng Yan^{1†}

¹*School of Physics and State Key Laboratory of Electronic Thin Films and Integrated Devices, University of Electronic Science and Technology of China, Chengdu 610054, China*

²*Institute for Advanced Study in Physics, Zhejiang University, Hangzhou 310027, China*

Significant progress has been made for the emerging concept of magnon frequency comb (MFC) but mainly in the classical region. The quantum property of the comb structure is yet to be explored. Here we theoretically investigate the quantum fluctuations of frequency combs and demonstrate the continuous-variable quantum entanglement and Einstein-Podolsky-Rosen (EPR) steering between different teeth of MFC. Without loss of generality, we address this issue in a hybrid magnon-skyrmion system. We observe a strong two-mode squeezed entanglement and asymmetric steering between the sum- and difference-frequency magnon teeth mediated by the skyrmion that acts as an effective reservoir to cool the Bogoliubov mode delocalized over the first-order magnon pair in MFC. Our findings show the prominent quantum nature of MFC, which has the potential to be utilized in ultrafast quantum metrology and multi-task quantum information processing.

I. INTRODUCTION

Magnon frequency comb (MFC) is a spin-wave (SW, with its quantum called magnon) spectrum composed of a series of equidistant and coherent narrow spectral lines. The concept of MFC is attracting many recent attentions because of both fundamental interest and potential application in high-precision frequency measurement, ultra-sensitive detection, and ultra-fast magnon devices with the analogy of the optical frequency comb [1–3]. It has been shown that the MFC can be generated by means of various nonlinear effects, such as the three- and four-magnon scattering [4, 5], magnetostriction [6, 7], magnon Kerr effect [8, 9], magnon-optical Brillouin scattering [10], etc. The frequency range of coherent peaks in MFC has been extended from gigahertz (GHz) in ferromagnets to terahertz (THz) in antiferromagnets [11–13], and the controllable MFC bridging these two frequency domains is theoretically suggested in synthetic ferrimagnets as well [14]. Xu *et al.* [15] experimentally achieved a MFC with up to 20 comb teeth by driving a giant mechanical resonance with a strong pump field. Lately, Wang *et al.* [16] reported a tunable and low-power MFC with more than 32 comb teeth by using exceptional points which enhance the nonlinear interaction between the pump-induced magnon mode and the Kittel mode. Liu [17] theoretically predicted an ultra-wideband MFC containing up to 400 comb teeth based on the dissipative coupling between the magnon and cavity photon, indicating that there exists still a large room for exploring MFC with dense teeth. It has been proposed that the nonreciprocal MFC can be generated in the dual-cavity magnonic system via the asymmetrical response of magnon-Kerr nonlinearity in two different microwave input directions [8]. More recently, Liang *et al.* [18] demonstrated an asymmetric MFC through the nonlinear interaction between the skyrmion and chiral SW in a hybrid magnon-waveguide/skyrmion structure.

Three-magnon scattering is the leading nonlinear effect in

magnon dynamics, which includes both the confluence and splitting processes [19]. However, it is normally weak in uniformly magnetized ferromagnets due to the weak dipolar interaction. Intriguingly, it is theoretically proposed that the MFC can be generated by enhancing the nonlinearity through the interaction between propagating magnons and topological magnetic textures, such as skyrmions [4], bimerons [13], vortices [20], and domain walls [21, 22]. It is worth noting that the magnetic skyrmion, a vortex-like structure with topological protection, holds great potential for future high-density information storage and robust spintronic devices owing to its advantages of nanoscale size, stable structure, convenient manipulation, and low energy consumption [23, 24]. From another perspective, the nonlinear magnon-skyrmion scattering is inherently a quantum parametric oscillation process that describes the cascaded down-conversion and sum-frequency generation, which may imply interesting quantum effects of comb teeth.

Quantum entanglement is one of the most exotic features of quantum mechanics, which can be traced back to the Einstein-Podolsky-Rosen (EPR) paradox about the argument on the completeness of quantum theory [25]. In response to this paradox, Schrödinger introduced entangled state and first proposed steering to describe the nonlocality of spooky action at a distance in EPR paradox [26]. In a system composed of two subsystems A and B, B can be controlled to the corresponding state by performing suitable measurements on A, which is called quantum steering [27]. Different from the quantum entanglement, the EPR steering has more stringent correlation condition and exhibits an intrinsic asymmetry, or even unidirectionality, that is to say, one party of the two subsystems can control the quantum state of the other one, but not vice versa [28, 29]. In the past few decades, quantum entanglement and steering as the key resources have played important roles in quantum computing [30], quantum cryptography [31], quantum sensing [32], quantum teleportation [33], and quantum key distribution [34, 35]. Although quantum correlations between magnons and various quasi-particles have been investigated [36–44], their manifestation among different magnon teeth in the emerging MFC is still an open issue.

* hyyuan@zju.edu.cn

† yan@uestc.edu.cn

In this work, we study the quantum correlations of spectral lines of MFC. Without loss of generality, we consider a coupled system consisting of a magnon waveguide and a magnetic skyrmion microresonator [see Fig. 1(a)]. The isolated magnetic skyrmion supporting a circular 180° domain wall can be treated as a microring resonator (the quality factor $Q \approx 10^4$) that allows the magnonic whispering gallery mode (mWGM). When the mWGM driven by a microwave field enters the microresonator along the waveguide, it can be nonlinearly coupled to the skyrmion mode (e.g., skyrmion breathing, gyration, or skyrmion-wall circling modes), leading to the generation of MFC. We find that there are two separate parameter regimes, one of which has a finite threshold while the other has a divergent threshold, depending on the model parameters. When the driving power is below the threshold, only the mWGM is macroscopically occupied. In such a case, the mWGM can be parametrically approximated as a classical state and it is decoupled from the skyrmion microresonator. For the case above the threshold, all magnon modes would be excited but their solutions exhibit phase shifts, which is induced by the strong nonlinearity [45] and makes the determination of the phases challenging. In this study, we only consider the quantum fluctuations of MFC below the threshold by the standard linearization procedure. It is found that the entanglement between the skyrmion mode and the difference-frequency mode originating from their two-mode squeezing interaction can be transferred to the sum- and difference-frequency modes. Intriguingly, the strong entanglement and asymmetric steering between the two magnons are mediated by the skyrmion which acts as an engineered reservoir to cool the delocalized Bogoliubov mode through the linear beam-splitter interaction. We show that one party with larger effective magnon number steers the other one, and the steering direction can be flexibly controlled by the magnon dissipations. We interpret the underlying mechanism by constructing an effective Hamiltonian, and discuss parameters in tuning the quantum entanglement and EPR steering. In experiments, the comb lines close to the pumped magnon mode will be significantly excited, while magnon modes far from the pump remain unoccupied macroscopically. Therefore, the above quantum correlation analysis based on the two-mode squeezed model is well applicable to modes away from the pump.

This paper is organized as follows. In Sec. II, we introduce the theoretical model to describe the nonlinear magnon-skyrmion interaction. The system Hamiltonian and the corresponding quantum Langevin equations (QLEs) are provided. In Sec. III, we give the stationary semi-classical solutions and analyze the linearized quantum fluctuation dynamics. The bipartite entanglement and quantum steering criteria are shown in Sec. IV. We then discuss the generation and manipulation of quantum correlation of the skyrmion and the magnon comb modes in Sec. V. The verification of two-mode squeezed entanglement of the first-order magnon pair with respect to the reconstructed Wigner function and the experimental measurement scheme of quantum entanglement and steering are given in Sec. VI. Conclusions are drawn in Sec. VII.

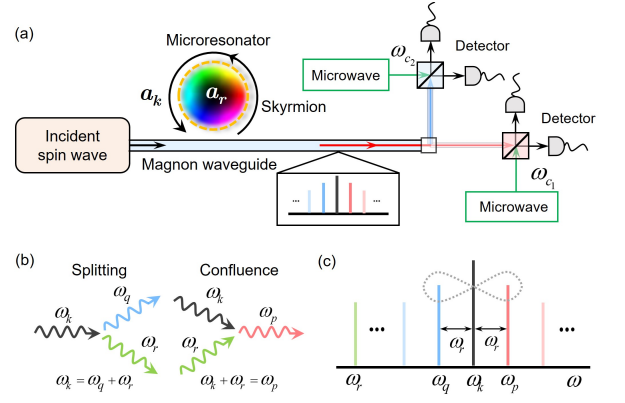


FIG. 1. (a) Schematic illustration of the magnon-skyrmion hybrid system for the generation of MFC and the measurement scheme of the quantum entanglement and steering. The driven SW propagating in a magnon waveguide is incident into a skyrmion microresonator, simultaneously stimulating the mWGM a_k with frequency ω_k , which can be coupled with the skyrmion mode a_r with frequency ω_r via the three-magnon process. Weak microwave fields with frequencies $\omega_{c1, c2}$ are sent to couple to the output MFC and the position and momentum of the magnon can be measured by homodyning the microwave field output. (b) Splitting and confluence processes of the nonlinear magnon-skyrmion scattering. (c) The spectrum of an ideal MFC is discrete, equally spaced, and wide-band, where the comb spacing is determined by the frequency of the skyrmion mode and different comb teeth can be entangled, labeled by the dotted figure-of-eight.

II. THEORETICAL MODEL

We consider a hybrid system composed of a magnon waveguide and a skyrmion microresonator that supports the mWGM, as shown in Fig. 1(a). The single magnetic skyrmion can be regarded as a microresonator because its magnetization rotates smoothly from the core down to the perimeter up, forming a circular 180° domain wall [46] that allows gapless SW excitations [18]. When the driving SW is injected into the skyrmion microresonator through the waveguide, a mWGM with the same frequency is excited. It is then split into a skyrmion mode and a difference-frequency mode via the three-magnon process, and the confluence between the mWGM and the skyrmion mode generates the sum-frequency mode, as shown in Fig. 1(b). The chain-like nonlinear processes finally induce the MFC [4]. Here, we focus on the possible quantum correlation among the skyrmion (ω_r) and lowest three MFC teeth ($\omega_k, \omega_p, \omega_q$), as depicted in Fig. 1(c). The Hamiltonian describing the nonlinear magnon-skyrmion interaction is written as ($\hbar = 1$)

$$\begin{aligned}
 H = & \omega_k a_k^\dagger a_k + \omega_r a_r^\dagger a_r + \omega_p a_p^\dagger a_p + \omega_q a_q^\dagger a_q \\
 & + g_p (a_k a_r a_p^\dagger + a_k^\dagger a_r^\dagger a_p) + g_q (a_k a_r^\dagger a_q^\dagger + a_k^\dagger a_r a_q) \\
 & + iE (a_k^\dagger e^{-i\omega_0 t} - a_k e^{i\omega_0 t}), \quad (1)
 \end{aligned}$$

where ω_k and ω_r are the resonant frequencies of the mWGM and the skyrmion mode, respectively, with a_k (a_k^\dagger) and a_r (a_r^\dagger) being their annihilation (creation) operators accord-

ingly. a_p (a_p^\dagger) and a_q (a_q^\dagger) are the annihilation (creation) operators of the sum- and difference-frequency magnons, respectively, whose frequencies satisfy $\omega_p = \omega_k + \omega_r$ and $\omega_q = \omega_k - \omega_r$. g_p and g_q are the nonlinear magnon-skyrmion coupling strengths, which are considered as real numbers for simplicity. The incident SW is driven by the microwave field with the frequency ω_0 and the amplitude E being the strength of the driving field.

In the rotating frame at the frequency ω_0 , the system Hamiltonian can be recast as

$$\begin{aligned} H = & \Delta_k a_k^\dagger a_k + \omega_r a_r^\dagger a_r + \Delta_p a_p^\dagger a_p + \Delta_q a_q^\dagger a_q \\ & + g_p (a_k a_r a_p^\dagger + a_k^\dagger a_r^\dagger a_p) + g_q (a_k a_r^\dagger a_q^\dagger + a_k^\dagger a_r a_q) \\ & + iE (a_k^\dagger - a_k), \end{aligned} \quad (2)$$

where $\Delta_{k(p,q)} = \omega_{k(p,q)} - \omega_0$. Considering the magnon dissipations and environmental noise, we derive the QLEs as follows

$$\begin{aligned} \dot{a}_k = & - (i\Delta_k + \kappa_k) a_k - ig_p a_r^\dagger a_p - ig_q a_r a_q + E \\ & + \sqrt{2\kappa_k} a_k^{\text{in}}, \\ \dot{a}_r = & - (i\omega_r + \kappa_r) a_r - ig_p a_k^\dagger a_p - ig_q a_k a_q^\dagger + \sqrt{2\kappa_r} a_r^{\text{in}}, \\ \dot{a}_p = & - (i\Delta_p + \kappa_p) a_p - ig_p a_k a_r + \sqrt{2\kappa_p} a_p^{\text{in}}, \\ \dot{a}_q = & - (i\Delta_q + \kappa_q) a_q - ig_q a_k a_r^\dagger + \sqrt{2\kappa_q} a_q^{\text{in}}, \end{aligned} \quad (3)$$

where κ_j ($j = k, r, p, q$) and a_j^{in} are the dissipation coefficient and the input noise operator of the corresponding magnon mode, respectively. Under the Markovian reservoir assumption, the input noise is characterized by the zero-mean correlation functions: $\langle a_j^{\text{in}}(t) a_j^{\text{in}\dagger}(t') \rangle = [\bar{n}_j(\omega_j) + 1] \delta(t - t')$, and $\langle a_j^{\text{in}\dagger}(t) a_j^{\text{in}}(t') \rangle = \bar{n}_j(\omega_j) \delta(t - t')$. The equilibrium mean thermal number of each mode is $\bar{n}_j(\omega_j) = [\exp(\hbar\omega_j/k_B T) - 1]^{-1}$, where T is the environmental temperature and k_B is the Boltzmann constant.

III. LINEARIZED QUANTUM FLUCTUATION ANALYSIS

When the system is at the steady state, the dynamics can be linearized by expressing the operators as the sum of their expectation values and quantum fluctuations $a_j = \langle a_j \rangle + \delta a_j$. The mean value solutions could be obtained from a set of semi-classical differential equations when $d\langle a_j \rangle/dt = 0$. In these cases we may use the linearized quantum fluctuation analysis to simplify the physical model, and further study quantum correlation among different modes.

Neglecting all fluctuations terms, the semi-classical equations for the magnon mean values are expressed as

$$\begin{aligned} \langle \dot{a}_k \rangle = & - (i\Delta_k + \kappa_k) \langle a_k \rangle - ig_p \langle a_r^\dagger \rangle \langle a_p \rangle - ig_q \langle a_r \rangle \langle a_q \rangle + E, \\ \langle \dot{a}_r \rangle = & - (i\omega_r + \kappa_r) \langle a_r \rangle - ig_p \langle a_k^\dagger \rangle \langle a_p \rangle - ig_q \langle a_k \rangle \langle a_q^\dagger \rangle, \\ \langle \dot{a}_p \rangle = & - (i\Delta_p + \kappa_p) \langle a_p \rangle - ig_p \langle a_k \rangle \langle a_r \rangle, \\ \langle \dot{a}_q \rangle = & - (i\Delta_q + \kappa_q) \langle a_q \rangle - ig_q \langle a_k \rangle \langle a_r^\dagger \rangle. \end{aligned} \quad (4)$$

For convenience, we write the driving field and steady-state mean value of the system in complex numbers $E = \varepsilon e^{i\phi_i}$ and $\langle a_j \rangle = A_j e^{i\phi_j}$. We find that the steady-state solutions are divided into two different classes depending on whether the threshold of the system driving field is finite or divergent.

If $g_q^2 \kappa_p > g_p^2 \kappa_q$, we find a threshold field amplitude

$$\varepsilon_{\text{th}} = \kappa_k \sqrt{\frac{\kappa_r \kappa_p \kappa_q}{g_q^2 \kappa_p - g_p^2 \kappa_q}}, \quad (5)$$

with $\Delta_k = 0$. Below the threshold, only the mWGM matching the driving frequency ω_0 is resonantly excited while other magnons will not be macroscopically occupied. In this circumstance, the steady-state solutions can be obtained

$$\langle a_k \rangle = E/\kappa_k, \langle a_r \rangle = \langle a_p \rangle = \langle a_q \rangle = 0. \quad (6)$$

When the pumping amplitude ε is above the threshold, there exist another steady-state solution of the mWGM, skyrmion, sum- and difference-frequency magnon modes as

$$\begin{aligned} \langle a_k \rangle = & \sqrt{\frac{\kappa_r \kappa_p \kappa_q}{g_q^2 \kappa_p - g_p^2 \kappa_q}} e^{i\phi_k}, \\ \langle a_r \rangle = & \sqrt{\frac{(\varepsilon - \varepsilon_{\text{th}}) \kappa_k \kappa_p \kappa_q}{\varepsilon_{\text{th}} (g_q^2 \kappa_p + g_p^2 \kappa_q)}} e^{i\phi_r}, \\ \langle a_p \rangle = & g_p \kappa_q \sqrt{\frac{(\varepsilon - \varepsilon_{\text{th}}) \kappa_k \kappa_r}{\varepsilon_{\text{th}} (g_q^4 \kappa_p^2 - g_p^4 \kappa_q^2)}} e^{i\phi_p}, \\ \langle a_q \rangle = & g_q \kappa_p \sqrt{\frac{(\varepsilon - \varepsilon_{\text{th}}) \kappa_k \kappa_r}{\varepsilon_{\text{th}} (g_q^4 \kappa_p^2 - g_p^4 \kappa_q^2)}} e^{i\phi_q}, \end{aligned} \quad (7)$$

where the phases satisfy $\phi_k = \phi_l$, $\phi_p + \phi_q = 2\phi_k + \pi$, $\phi_p - \phi_q = 2\phi_r$. The only phase we know here is the phase of the driving field E . If we take E as a real number, $\langle a_k \rangle$ will also be a real number. But other phases $\phi_{r,p,q}$ are not fixed, which indicates phase shifts of these solutions above the threshold [45], that is, they are uncertain.

If $g_q^2 \kappa_p \leq g_p^2 \kappa_q$, the threshold diverges, which implies that no matter how strong the pump field is, other magnon modes will not be macroscopically occupied. The expressions of the stationary solutions are then the same as Eq. (6).

In what follows, we shall only investigate the quantum correlation for model parameters allowing the steady-state solutions (6). Based on Eq. (3), we can linearize the fluctuations around the steady state, and obtain

$$\begin{aligned} \delta \dot{a}_k = & - (i\Delta_k + \kappa_k) \delta a_k - ig_p \langle a_r^\dagger \rangle \delta a_p - ig_p \langle a_p \rangle \delta a_r^\dagger \\ & - ig_q \langle a_r \rangle \delta a_q - ig_q \langle a_q \rangle \delta a_r + \sqrt{2\kappa_k} \delta a_k^{\text{in}}, \\ \delta \dot{a}_r = & - (i\omega_r + \kappa_r) \delta a_r - ig_p \langle a_k^\dagger \rangle \delta a_p - ig_p \langle a_p \rangle \delta a_k^\dagger \\ & - ig_q \langle a_k \rangle \delta a_q^\dagger - ig_q \langle a_q^\dagger \rangle \delta a_k + \sqrt{2\kappa_r} \delta a_r^{\text{in}}, \\ \delta \dot{a}_p = & - (i\Delta_p + \kappa_p) \delta a_p - ig_p \langle a_k \rangle \delta a_r - ig_p \langle a_r \rangle \delta a_k \\ & + \sqrt{2\kappa_p} \delta a_p^{\text{in}}, \\ \delta \dot{a}_q = & - (i\Delta_q + \kappa_q) \delta a_q - ig_q \langle a_k \rangle \delta a_r^\dagger - ig_q \langle a_r^\dagger \rangle \delta a_k \\ & + \sqrt{2\kappa_q} \delta a_q^{\text{in}}. \end{aligned} \quad (8)$$

By introducing the magnons position and momentum quadrature fluctuation operators $X_j = (\delta a_j + \delta a_j^\dagger)/\sqrt{2}$, $Y_j = i(\delta a_j^\dagger - \delta a_j)/\sqrt{2}$, and the input noise quadrature operators $X_j^{\text{in}} = (\delta a_j^{\text{in}} + \delta a_j^{\text{in}\dagger})/\sqrt{2}$, $Y_j^{\text{in}} = i(\delta a_j^{\text{in}\dagger} - \delta a_j^{\text{in}})/\sqrt{2}$, the linearized QLEs describing the quantum fluctuations can be recast as

$$\dot{\mathbf{u}}(t) = \mathbf{M}\mathbf{u}(t) + \mathbf{n}(t), \quad (9)$$

where the vector of quadrature operators $\mathbf{u}(t) = [\delta X_k(t), \delta Y_k(t), \delta X_r(t), \delta Y_r(t), \delta X_p(t), \delta Y_p(t), \delta X_q(t), \delta Y_q(t)]^T$, the vector of noise operators $\mathbf{n}(t) = [\sqrt{2\kappa_k}X_k^{\text{in}}, \sqrt{2\kappa_k}Y_k^{\text{in}}, \sqrt{2\kappa_r}X_r^{\text{in}}, \sqrt{2\kappa_r}Y_r^{\text{in}}, \sqrt{2\kappa_p}X_p^{\text{in}}, \sqrt{2\kappa_p}Y_p^{\text{in}}, \sqrt{2\kappa_q}X_q^{\text{in}}, \sqrt{2\kappa_q}Y_q^{\text{in}}]^T$, and M is the drift matrix. If the real parts of all eigenvalues of M are negative, the system is stable and reaches a steady state, known as the Routh-Hurwitz criterion [47]. Because the dynamics of quadrature components fluctuations are linearized and the input noises are Gaussian, the system finally evolves into a zero-mean continuous variable (CV) Gaussian state that can be characterized by a 8×8 covariance matrix (CM) V , where the matrix elements are defined as $V_{kl} = \langle \mathbf{u}_k(\infty)\mathbf{u}_l(\infty) + \mathbf{u}_l(\infty)\mathbf{u}_k(\infty) \rangle / 2$ ($k, l = 1, 2, \dots, 8$). From Eq. (9), the formal solution of the linearized QLEs is given by $\mathbf{u}(t) = \mathbf{\Lambda}(t)\mathbf{u}(0) + \int_0^t ds \mathbf{\Lambda}(s)\mathbf{n}(t-s)$ with $\mathbf{\Lambda}(t) = \exp(\mathbf{M}t)$. In the steady state $t \rightarrow \infty$, one acquires $\mathbf{\Lambda}(\infty) = 0$ and $\mathbf{u}_k(\infty) = \int_0^\infty ds \sum_i \mathbf{\Lambda}_{ki}(s)\mathbf{n}(t-s)$. Based on the fact that the eight components of $\mathbf{n}(t)$ are uncorrelated with each other, one gets $V = \int_0^\infty ds \mathbf{\Lambda}(s)D\mathbf{\Lambda}^T(s)$, where D is the diffusion matrix defined as $D_{kl}\delta(s-s') = \langle \mathbf{n}_k(s)\mathbf{n}_l(s') + \mathbf{n}_l(s')\mathbf{n}_k(s) \rangle / 2$. When the system stability conditions are fulfilled, the steady-state CM V can be obtained by solving the Lyapunov equation [48]

$$MV + VM^T = -D. \quad (10)$$

The CM V is a real and symmetric matrix and must satisfy the Robertson-Schrödinger uncertainty relation [49, 50] $V + i\Omega_n > 0$, which is the necessary and sufficient condition for the Gaussian state to be physical and implies the positive definiteness $V > 0$. $\Omega_n = \oplus_{j=1}^n i\sigma_y$ is the standard symplectic form (σ_y is the y -Pauli matrix). With the CM V , one can analyze the entanglement properties among magnons with different frequencies in MFC at the steady state.

IV. ENTANGLEMENT AND STEERING CRITERIA

To quantitatively study the quantum correlation of magnons in the multipartite CV system, we adopt the logarithmic negativity E_N [51] to calculate the bipartite entanglement, which is defined as

$$E_N = \max[0, -\ln(2\nu)], \quad (11)$$

where $\nu = \sqrt{\sum(\tilde{V}) - [\sum(\tilde{V})^2 - 4 \det \tilde{V}]^{1/2}} / \sqrt{2}$ is the minimal symplectic eigenvalue of the partial transpose of a reduced 4×4 CM \tilde{V} with $\sum(\tilde{V}) \equiv \det(V_1) + \det(V_2) - 2 \det(V_{12})$. The reduced CM \tilde{V} of two selected modes under consideration can

be obtained by tracing out the rows and columns of the uninteresting modes in V , which is given by

$$\tilde{V} = \begin{pmatrix} V_1 & V_{12} \\ V_{12}^T & V_2 \end{pmatrix}, \quad (12)$$

where V_1 and V_2 are 2×2 block matrices corresponding to modes 1 and 2, respectively. If $E_N > 0$, namely, $\nu < 1/2$, the considered bipartition are entangled, which is equivalent to the Peres-Horodecki criterion for certifying bipartite entanglement of Gaussian states [52], and the larger E_N the higher the degree of entanglement. Besides, the Gaussian quantum steering can be calculated quantitatively by [53]

$$S_{12} = \max\{0, S(2V_1) - S(2\tilde{V})\}, \\ S_{21} = \max\{0, S(2V_2) - S(2\tilde{V})\}, \quad (13)$$

where $S(\sigma) = [\ln \det(\sigma)] / 2$. A nonzero $S_{12} > 0$ ($S_{21} > 0$) denotes that the bipartite Gaussian state is steerable from mode 1 (2) to mode 2 (1) by applying Gaussian measurements on mode 1 (2), and the larger of its value denotes the stronger Gaussian steerability. Moreover, the directionality of quantum steering could be better analyzed by introducing the effective magnon number, which can be calculated through the diagonal elements of the CM V from

$$N_j = [\langle \delta X_j^2 \rangle + \langle \delta Y_j^2 \rangle - 1] / 2, \quad (14)$$

with j labeling the magnon mode.

V. RESULTS AND DISCUSSION

In this section, we will demonstrate the quantum entanglement and EPR steering among the skyrmion mode and teeth of MFC. When the hybrid magnon-skyrmion system is resonantly driven with $\Delta_k = 0$, the solution of $\langle a_k \rangle$ is given by a real number E/κ_k by assuming $\phi_k = 0$. From Eq. (8), the QLEs of fluctuations are reduced to

$$\delta \dot{a}_k = -\kappa_k \delta a_k + \sqrt{2\kappa_k} \delta a_k^{\text{in}}, \\ \delta \dot{a}_r = -(i\omega_r + \kappa_r) \delta a_r - iG_p \delta a_p - iG_q \delta a_q^\dagger + \sqrt{2\kappa_r} \delta a_r^{\text{in}}, \\ \delta \dot{a}_p = -(i\omega_r + \kappa_p) \delta a_p - iG_p \delta a_r + \sqrt{2\kappa_p} \delta a_p^{\text{in}}, \\ \delta \dot{a}_q = (i\omega_r - \kappa_q) \delta a_q - iG_q \delta a_r^\dagger + \sqrt{2\kappa_q} \delta a_q^{\text{in}}, \quad (15)$$

where $G_p = g_p \langle a_k \rangle$ and $G_q = g_q \langle a_k \rangle$ are effective coupling strengths describing the confluence and splitting processes, respectively. Equations (15) show that the mWGM is decoupled from the rest system, so we will focus on the fluctuation dynamics of the skyrmion, the sum- and difference-frequency magnons next. The corresponding drift matrix M is given by

$$M = \begin{pmatrix} -\kappa_r & \omega_r & 0 & G_p & 0 & -G_q \\ -\omega_r & -\kappa_r & -G_p & 0 & -G_q & 0 \\ 0 & G_p & -\kappa_p & \omega_r & 0 & 0 \\ -G_p & 0 & -\omega_r & -\kappa_p & 0 & 0 \\ 0 & -G_q & 0 & 0 & -\kappa_q & -\omega_r \\ -G_q & 0 & 0 & 0 & \omega_r & -\kappa_q \end{pmatrix}. \quad (16)$$

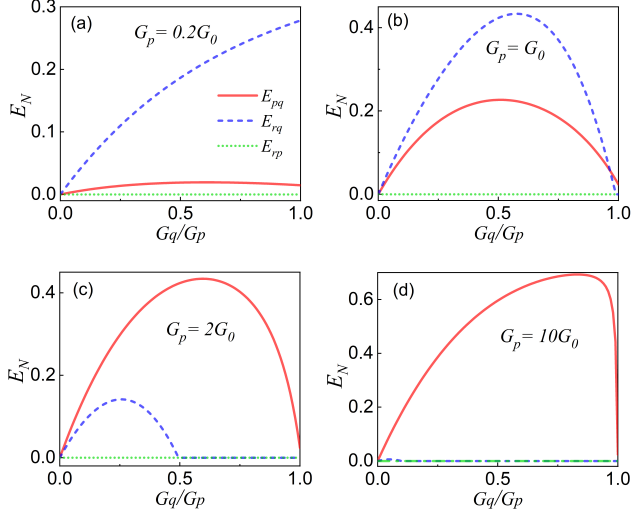


FIG. 2. Logarithmic negativity of bipartite entanglements E_{rp} , E_{rq} and E_{pq} versus the ratio of coupling strengths G_q/G_p for (a) $G_p = 0.2G_0$, (b) $G_p = G_0$, (c) $G_p = 2G_0$, and (d) $G_p = 10G_0$ with $G_0/2\pi = 15$ MHz.

Correspondingly, $\mathbf{u}(t) = [\delta X_r(t), \delta Y_r(t), \delta X_p(t), \delta Y_p(t), \delta X_q(t), \delta Y_q(t)]^T$, $\mathbf{n}(t) = [\sqrt{2\kappa_r}X_r^{\text{in}}, \sqrt{2\kappa_r}Y_r^{\text{in}}, \sqrt{2\kappa_p}X_p^{\text{in}}, \sqrt{2\kappa_p}Y_p^{\text{in}}, \sqrt{2\kappa_q}X_q^{\text{in}}, \sqrt{2\kappa_q}Y_q^{\text{in}}]^T$, and $D = \text{diag}[\kappa_r(2\bar{n}_a + 1), \kappa_r(2\bar{n}_a + 1), \kappa_p(2\bar{n}_p + 1), \kappa_p(2\bar{n}_p + 1), \kappa_q(2\bar{n}_q + 1), \kappa_q(2\bar{n}_q + 1)]$. We can obtain the effective Hamiltonian for the quantum fluctuation operators as follows

$$H_{\text{eff}} = \omega_r(\delta a_r^\dagger \delta a_r + \delta a_p^\dagger \delta a_p - \delta a_q^\dagger \delta a_q) + G_q(\delta a_r^\dagger \delta a_q^\dagger + \delta a_r \delta a_q) + G_p(\delta a_r^\dagger \delta a_p + \delta a_r \delta a_p^\dagger). \quad (17)$$

To calculate the steady-state bipartite entanglements among different magnon modes, we adopt the following parameters [4]: $\omega_k/2\pi = 80$ GHz, $\omega_r/2\pi = 8$ GHz, $\omega_p/2\pi = 88$ GHz, $\omega_q/2\pi = 72$ GHz, $\kappa_p/2\pi = \kappa_q/2\pi = 10$ MHz, $k_r/2\pi = 1$ MHz, and $T = 20$ mK. Figure 2 show the logarithmic negativity of the three bipartite cases versus the effective coupling ratio G_q/G_p for $G_p = 0.2G_0$, $G_p = G_0$, $G_p = 2G_0$, and $G_p = 20G_0$ with $G_0/2\pi = 15$ MHz, respectively. From Fig. 2(a), it can be found that the skyrmion mode and the difference-frequency mode are entangled ($E_{rq} > 0$), and the entanglement degree increases with the enhancement of the coupling of the magnon splitting process G_q . The weak entanglement between a_p and a_q also exists, but the skyrmion and the sum-frequency magnon are disentangled ($E_{rp} = 0$). The entanglement between a_p and a_q is significantly enhanced for a stronger G_p , as illustrated in Fig. 2(b). And it can be seen that the entanglement between the skyrmion and the difference-frequency magnon is nonmonotonic with the increase of the coupling ratio G_q , and it disappears with the parameter $G_q = G_p$ (dashed blue curve). When the effective coupling G_p is enhanced to $G_p = 2G_0$, the degree of the entanglement between two magnons E_{pq} is larger than that of the skyrmion-magnon entanglement E_{rq} in Fig. 2(c). And it is

obvious that the entanglement E_{rq} only exists in the parameter interval $G_q < 0.5G_p$. From Fig. 2(d), we can see that there is a strong entanglement between a_p and a_q , while the skyrmion mode (a_r) and the magnon mode (a_q) can hardly be entangled for a very large effective coupling $G_p = 10G_0$. Because the effective coupling strengths of the magnon-skyrmion interaction are directly proportional to the driving power of microwave field, it is not difficult to enhance $G_{p(q)}$ by 1~2 orders of magnitude. It is evident that this system has a sort of entanglement transfer (or sharing). One can interpret the physical mechanism via the effective Hamiltonian. With respect to the rotating frame at ω_r , the effective Hamiltonian can be written as $H'_{\text{eff}} = G_q(\delta a_r^\dagger \delta a_q^\dagger + \delta a_r \delta a_q) + G_p(\delta a_r^\dagger \delta a_p + \delta a_r \delta a_p^\dagger)$. We know that the first term is the parametric down-conversion (two-mode squeezed) coupling, which can entangle the skyrmion and the difference-frequency magnon. The second term is the linear beam-splitter coupling that generally does not create entanglement, but the entanglement can be partially transferred by means of such state exchange interaction, which leads to the entanglement between the sum- and difference-frequency magnon modes.

Figure 3 reveals the influence of the skyrmion dissipation on bipartite entanglements for different effective coupling strength G_p with the optimal coupling ratio G_q/G_p that corresponds to the maximum entanglement value. From Fig. 3(a), we observe that the steady-state entanglement gradually decreases with the increase of dissipation, showing a destructive role played by the skyrmion dissipation in the entanglement. However, a large enough dissipation would significantly enhance the entanglement of two magnon modes a_p and a_q with a strong coupling $G_p = 10G_0$, as shown in Fig. 3(b). And the stronger entanglement can be obtained under the greater effective coupling with the optimized coupling ratio. Here, the generation of entanglement between two magnons under the condition of strong magnon-skyrmion interaction satisfies the mechanism of reservoir engineering [54]. To demonstrate this point, we introduce two delocalized Bogoliubov modes β_1 and β_2

$$\begin{aligned} \beta_1 &= a_q \cosh \xi + a_p^\dagger \sinh \xi = S(\xi) a_q S^\dagger(\xi), \\ \beta_2 &= a_p \cosh \xi + a_q^\dagger \sinh \xi = S(\xi) a_p S^\dagger(\xi), \end{aligned} \quad (18)$$

where $S(\xi) = \exp[\xi(a_q a_p - a_q^\dagger a_p^\dagger)]$ is the two-mode squeezing operator with the effective squeezing parameter $\xi = \text{arctanh}(G_q/G_p)$. The system Hamiltonian (17) can be rewritten as (δ is omitted) $H_B = \omega_r(a_r^\dagger a_r + \beta_2^\dagger \beta_2 - \beta_1^\dagger \beta_1) + \tilde{G}(a_r^\dagger \beta_2 + a_r \beta_2^\dagger)$ with $\tilde{G} = \sqrt{G_p^2 - G_q^2}$. It turns out that the mode β_1 completely decouples with the skyrmion, and the mode β_2 has a beam-splitter type interaction with the skyrmion mode a_r . The squeezing operator $S(\xi)$ acts on the two-mode vacuum state $|0_p, 0_q\rangle$ and generates the two-mode squeezed vacuum state $|\xi\rangle = S(\xi)|0_p, 0_q\rangle$, which is the joint vacuum state of β_1 and β_2 and is also a two-mode entanglement state. Therefore, the entanglement can be obtained by cooling the Bogoliubov modes β_1 and β_2 to their ground state. In our work, only the β_2 mode is cooled by skyrmion that can be regarded as an engineered reservoir via the beam-splitter interaction, but the

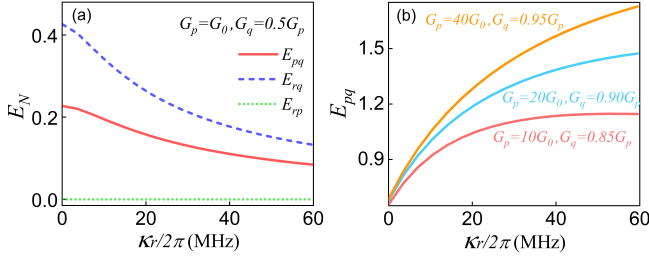


FIG. 3. (a) Logarithmic negativity of bipartite entanglements E_{rp} , E_{rq} and E_{pq} versus the dissipation rate of skyrmion κ_r with $G_p = G_0$, and $G_q = 0.5G_p$. (b) Bipartite entanglement E_{pq} versus the dissipation rate of skyrmion κ_r for different effective coupling strengths. Other parameters are the same as those in Fig. 2.

strong entanglement between a_p and a_q could still be realized. The cooling process is considered to be the predominant absorption of the Bogoliubov β_2 mode, which is eventually dissipated into the environment through the skyrmion leakage. The underlying state transition between the states of the skyrmion and Bogoliubov β_2 modes is $|n_s, m_{\beta_2}\rangle \leftrightarrow |n_s + 1, m_{\beta_2} - 1\rangle$ controlled by the interaction term in H_B , yet the dissipation process of the skyrmion does not change the Bogoliubov β_2 mode state with the transition $|n_s + 1, m_{\beta_2} - 1\rangle \rightarrow |n_s, m_{\beta_2} - 1\rangle$, where the skyrmion carries away the gained energy from the Bogoliubov β_2 mode, leading to its cooling. Similar physical mechanism has been utilized in hybrid cavity optomechanical and cavity magnonic systems to generate and manipulate the strong quantum correlation [55–59].

As a strict subset of quantum entanglement, the EPR steering plays an important role in one side device-independent quantum key distribution because of its inherent directionality. Below we discuss the EPR steering between magnon modes a_p and a_q . In Fig. 4, we can see that the steering can be strengthened by increasing the skyrmion dissipation κ_r , whereas they first increase and then decrease with the increase of G_q , and this nonmonotonic trend is similar to that of the entanglement curve in Fig. 2(d). On the one hand, enhancing G_q for a fixed G_p increases the squeezing parameter ξ , which leads to the enhancement of entanglement. On the other hand, the occupancies of the Bogoliubov modes $\langle \beta_{1(2)}^\dagger \beta_{1(2)} \rangle = \cosh^2 \xi \langle a_{q(p)}^\dagger a_{q(p)} \rangle + \sinh^2 \xi \langle a_{p(q)}^\dagger a_{p(q)} \rangle + \sinh \xi \cosh \xi \langle a_q a_p^\dagger + a_q^\dagger a_p \rangle$ become exponentially large with the increase of ξ where $\langle a_{p(q)}^\dagger a_{p(q)} \rangle$ is the thermal magnon number, and the cooling effect of the skyrmion is suppressed due to the effective coupling \tilde{G} decreasing with increasing G_q , thus the quantum correlation is weakened. Comparing Fig. 4(a) with Fig. 4(b), it can be seen that the asymmetric steering between the two magnons emerges. We observe that the bipartite steering parameter S_{qp} is always larger than S_{pq} . It indicates that applying Gaussian measurements on a_p or a_q mode could bidirectionally steer the state of the other mode, yet the steerability of a_q is stronger than that of a_p . It is worth noting that the asymmetric steering is intrinsic in our system, which does not require imposed unbalanced losses or noises

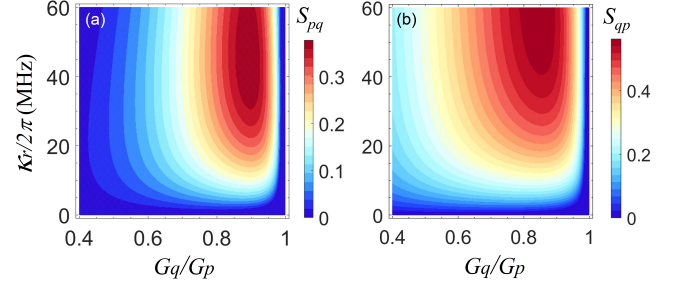


FIG. 4. Density plot of the asymmetric EPR steering (a) S_{pq} and (b) S_{qp} versus the ratio of coupling strengths G_q/G_p and the dissipation rate of skyrmion focus on with $G_p = 10G_0$ and $\kappa_r/2\pi = 40$ MHz.

on two parties at the expense of reduced steerability.

Additionally, the steering direction could be performed in a controllable manner by changing the dissipation rates of a_p and a_q . The asymmetric external environments of two magnons can cause asymmetric quantum correlation that is beneficial for achieving the one-way steering. The stationary entanglement and steering of two magnons as functions of the dissipation ratio κ_q/κ_p with a fixed $\kappa_p/2\pi = 10$ MHz are displayed on Fig. 5(a), and the regions of two-way (blue and red), one-way (green), and no-way (yellow) EPR steering are respectively indicated by different colors. It is found that the correlation of two-magnon entanglement is always larger than the quantum steering for the same parameters regime ($E_{pq} > S_{pq}, S_{qp}$). Both the entanglement and steering decrease with the increase of κ_q/κ_p , which indicates that the magnon damping is destructive to the quantum correlation between two magnons. In the parameter regime $\kappa_q/\kappa_p < 2$, there is a bidirectional steering, in which the steering directions of the two magnons are competitive. With the increase of κ_q/κ_p , S_{qp} is larger than S_{pq} , indicating a stronger steerable ability from the q -mode to p -mode with the parameters regime $\kappa_q/\kappa_p < 1.5$ (blue region). However, when the dissipation ratio falls into the region $1.5 < \kappa_q/\kappa_p < 2.1$, the steering direction is reversed and the steerability from the p -mode to the q -mode is dominant ($S_{qp} < S_{pq}$, red region). An intuitive picture is as follows: the large κ_q/κ_p means that the interaction between the q -mode and its thermal bath is stronger than that between the p -mode and its bath, resulting in the steering S_{pq} dropping faster than the steering S_{qp} . In other words, the magnon mode with a larger damping is more difficult to steer the other one. Obviously, the one-way steering from the p -mode to the q -mode appears when the dissipation ratio satisfies $2.1 < \kappa_q/\kappa_p < 2.3$, where applying Gaussian measurements on the p -mode could unidirectionally steer the q -mode but not vice versa. As κ_q/κ_p continues to increase, both steering S_{qp} and S_{pq} disappear completely, but the magnon entanglement still exists, which is attributed to the stricter quantum correlation of steering than that of entanglement.

The effective magnon number of p - and q -modes closely related to the directionality of EPR steering versus the dissipation ratio κ_q/κ_p are plotted in Fig. 5(b). Compared with Fig. 5(a), it is evident that one mode with a larger population has

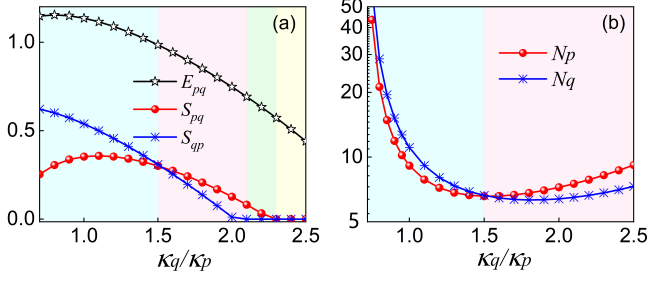


FIG. 5. (a) Bipartite entanglement E_{pq} , bipartite steering S_{pq} , and S_{qp} versus the ratio of dissipation rate κ_q/κ_p with $G_p = 10G_0$ MHz, $G_q = 0.85G_p$, $\kappa_p/2\pi = 10$ MHz, and $\kappa_r/2\pi = 40$ MHz. (b) The effective magnon numbers N_p and N_q versus the ratio of dissipation rate κ_q/κ_p .

more advantages in steering the other mode. The parameter region $N_q > N_p$ corresponds to the steering from the q -mode to the p -mode with $S_{qp} > S_{pq}$, and the reversal of the steering direction that from the p -mode to the q -mode corresponds to $N_q < N_p$. The populations of the two modes are equal for the bidirectionally symmetric steering at $\kappa_q/\kappa_p \approx 1.5$.

The entanglement and steering between p - and q -modes as functions of the environment temperature for $G_q = 10G_0$ and $G_q = 40G_0$ are illustrated in Fig. 6. It shows that the thermal noise would degrade the quantum correlation and meanwhile the steering is more sensitive to the temperature than the entanglement. From Fig. 6(a), we can see that the entanglement is robust against the thermal fluctuation, which can survive up to $T \approx 2.5$ K for $G_q = 10G_0$. The asymmetric steering is reasonably robust against temperature when $T < 0.9$ K, and the ability of the q -mode to steer the p -mode is always larger than the other way around (i.e., $S_{qp} > S_{pq}$). As shown in Fig. 6(b), the survival temperature of entanglement can be extended to 4.5 K under a stronger effective coupling $G_q = 40G_0$. Similarly, it is obvious that the degree of two-way steering and its robustness against temperature could be significantly improved, and the asymmetric steering even exists above 2 K. Theoretically, if the resonance frequency of magnons can be increased to the THz range such as in antiferromagnets, the preparation and manipulation of entanglement can work at a temperature of several tens of Kelvin. Since the THz MFC has been theoretically predicted [11–13], we envision that our results can be extended to the antiferromagnetic systems in a straightforward way.

VI. VERIFICATION AND MEASUREMENT OF QUANTUM ENTANGLEMENT

From the above analysis, it can be found that the first-order frequency comb teeth produce two-mode squeezed entanglement under the condition of strong effective magnon-skyrmion coupling. To verify the quantum correlation, the two-mode squeezed quadratures of the sum- and difference-frequency magnon modes in the phase space are more in-

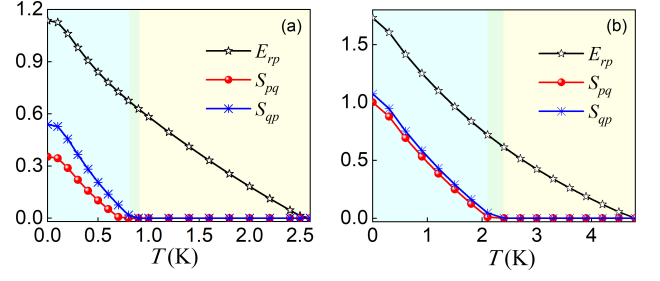


FIG. 6. Bipartite entanglement E_{pq} , bipartite steering S_{pq} , and S_{qp} versus temperature T for different effective coupling strengths (a) $G_p = 10G_0$, $G_q = 0.85G_p$, and $\kappa_r/2\pi = 40$ MHz, and (b) $G_p = 40G_0$, $G_q = 0.95G_p$, and $\kappa_r/2\pi = 60$ MHz.

tuitively visualized in terms of the quasiprobability Wigner functions. Because the steady state of the coupled system belongs to the Gaussian state class, its reconstructed Wigner function $W(\mu_{pq})$ can be characterized by a multivariate normal distribution, which is defined as

$$W(\mu_{pq}) = \frac{\exp(-\frac{1}{2}\mu_{pq}V_{pq}^{-1}\mu_{pq}^T)}{\pi^2\sqrt{\det(V_{pq})}}, \quad (19)$$

where $\mu_{pq} = (\delta X_p, \delta Y_p, \delta X_q, \delta Y_q)$. Figure 7 shows the reconstructed Wigner function of different quadrature pairs. Note that when the boundary of the solid black ellipse enters into the dashed gray circle, it indicates the existence of a squeezed state, where the variance of the relevant steady state is smaller than that of a vacuum state. It can be seen that the marginals from the same quadratures $(\delta X_p, \delta Y_p)$ and $(\delta X_q, \delta Y_q)$ show unsqueezed thermal noise above the vacuum noise. The cross-quadrature marginals $(\delta X_p, \delta X_q)$ and $(\delta Y_p, \delta Y_q)$ show two-mode squeezing in the diagonal and off-diagonal directions, which indicates that two-mode squeezed correlation appear for the associated magnons. The generated two-mode squeezing could be applied in the CV quantum processing and the quantum-enhanced measurement [60–62].

Lastly, we discuss the experimental scheme to measure the generated quantum entanglement and steering of MFC. The quantization of bipartite quantum correlation E_N and $S_{12(21)}$ can be obtained via measuring the elements of the CM V at the steady state. The method of measuring the magnon is analogous to the mechanical oscillator. It has been experimentally realized for the case of entangled mechanical modes with the help of the microwave probe technique [63, 64]. As shown in Fig. 1(a), two weak microwave fields are sent to be resonantly coupled with magnons with different frequencies in the output MFC. The quantum state of the magnon is efficiently transferred to the microwave photon via the linear beam-splitter interaction. Therefore, the position and momentum of the magnon mode can be read by the homodyne detection of the output microwave mode. The relevant dynamics of the magnon-microwave interaction can be described by [48]

$$\delta\dot{c} = -\kappa_c\delta c - ig\delta a + \sqrt{2\kappa_c}\delta c^{\text{in}}, \quad (20)$$

where κ_c and δc^{in} are the dissipation and the input noise of

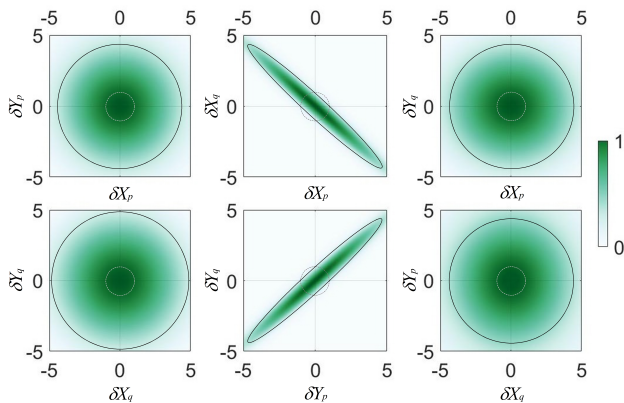


FIG. 7. Reconstructed Wigner functions of different quadrature pairs. The solid black (dashed gray) line represents the $1/e$ fall-off from the maximum value of $W(\mu_{pq})$ for the relevant steady state (vacuum) of the corresponding subsystem. $G_p = 10G_0$, $G_q = 0.85G_p$, $\kappa_r/2\pi = 40$ MHz, and other parameters are in the text.

microwave, respectively, and g is the magnon-microwave coupling strength. When the microwave dissipation $\kappa_c \gg g$, the microwave mode adiabatically follows the magnon dynamics. From the input-output relationship [65] $c^{\text{out}} = \sqrt{2\kappa_c}c - c^{\text{in}}$, we get

$$\delta c^{\text{out}} = \frac{-i\sqrt{2}g}{\sqrt{\kappa_c}}\delta a + \delta c^{\text{in}}. \quad (21)$$

It indicates that the measurement of the output microwave give the magnon dynamics, and then all elements of V can be determined by measuring the correlations between the two microwave outputs, which allows one to determine both the quantum entanglement and steering.

VII. CONCLUSION

In conclusion, we have investigated the bipartite quantum correlation between different teeth of the MFC in a hybrid magnon-skyrmion system. We showed that the entanglement between the first-order comb lines can be generated, which originates from the transfer of the entanglement between the skyrmion mode and the difference-frequency magnon mode. The strong entanglement and asymmetric steering between the sum- and difference-frequency magnon modes can be obtained by controlling the magnon-skyrmion coupling strength and the skyrmion dissipation. The steering directionality could be manipulated by tuning the dissipation rates of two magnon modes, and the one-way EPR steering can be achieved at the steady state. We found that both the bipartite entanglement and steering are robust against thermal fluctuations, and their correlation and survival temperature could be significantly improved by enhancing the driving microwave field or by extending the working frequency of MFC to the THz region. Our work reveals the fundamental quantum entanglement and EPR steering of MFC, which could have potential applications in enhancing quantum precision measurement and multiparty quantum teleportation networks. The generalization of current work to higher-order comb teeth and multipartite cases is an open issue for future study.

ACKNOWLEDGMENTS

This work was funded by the National Key R&D Program under Contract No. 2022YFA1402802 and the National Natural Science Foundation of China (NSFC) (Grants No. 12374103, No. 12434003, and No. 12074057).

-
- [1] S. T. Cundiff and J. Ye, Colloquium: Femtosecond optical frequency combs, *Rev. Mod. Phys.* **75**, 325 (2003).
 - [2] N. Picqué and T. W. Hänsch, Frequency comb spectroscopy, *Nat. Photon.* **13**, 146 (2019).
 - [3] T. Fortier and E. Baumann, 20 years of developments in optical frequency comb technology and applications, *Commun. Phys.* **2**, 153 (2019).
 - [4] Z. Wang, H. Yuan, Y. Cao, Z.-X. Li, R. A. Duine, and P. Yan, Magnonic frequency comb through nonlinear magnonskyrmion scattering, *Phys. Rev. Lett.* **127**, 037202 (2021).
 - [5] T. Hula, K. Schultheiss, F. J. T. Gonçalves, L. Körber, M. Bejarano, M. Copus, L. Flacke, L. Liensberger, A. Buzdakov, A. Kákay, M. Weiler, R. Camley, J. Fassbender, and H. Schultheiss, Spin-wave frequency combs, *Appl. Phys. Lett.* **121**, 112404 (2022).
 - [6] H. Xiong, Magnonic frequency combs based on the resonantly enhanced magnetostrictive effect, *Fundam. Res.* **3**, 8 (2023).
 - [7] Z.-X. Liu, J. Peng, and H. Xiong, Generation of magnonic frequency combs via a two-tone microwave drive, *Phys. Rev. A* **107**, 053708 (2023).
 - [8] X. Wang, K.-W. Huang, Q.-Y. Qiu, and H. Xiong, Nonreciprocal double-carrier frequency combs in cavity magnonics, *Chaos Soliton. Fract.* **176**, 114137 (2023).
 - [9] J. Rao, B. Yao, C. Wang, C. Zhang, T. Yu, and W. Lu, Unveiling a pump-induced magnon mode via its strong interaction with walker modes, *Phys. Rev. Lett.* **130**, 046705 (2023).
 - [10] Z.-X. Liu and Y.-Q. Li, Optomagnonic frequency combs, *Photon. Res.* **10**, 2786 (2022).
 - [11] Z. Jin, X. Yao, Z. Wang, H. Yuan, Z. Zeng, W. Wang, Y. Cao, and P. Yan, Nonlinear topological magnon spin Hall effect, *Phys. Rev. Lett.* **131**, 166704 (2023).
 - [12] X. Yao, Z. Jin, Z. Wang, Z. Zeng, and P. Yan, Terahertz magnon frequency comb, *Phys. Rev. B* **108**, 134427 (2023).
 - [13] C. Zhang, Z. Jin, X. Liu, and P. Yan, Anisotropic magnon frequency comb based on antiferromagnetic bimerons, *Appl. Phys. Lett.* **125**, 052401 (2024).
 - [14] Y. Liu, T. Liu, Q. Yang, G. Tian, Z. Hou, D. Chen, Z. Fan, M. Zeng, X. Lu, X. Gao, et al., Design of controllable magnon frequency comb in synthetic ferrimagnets, *Phys. Rev. B* **109**, 174412 (2024).

- [15] G.-T. Xu, M. Zhang, Y. Wang, Z. Shen, G.-C. Guo, and C.-H. Dong, Magnonic frequency comb in the magnomechanical resonator, *Phys. Rev. Lett.* **131**, 243601 (2023).
- [16] C. Wang, J. Rao, Z. Chen, K. Zhao, L. Sun, B. Yao, T. Yu, Y.-P. Wang, and W. Lu, Enhancement of magnonic frequency combs by exceptional points, *Nat. Phys.* **20**, 1139 (2024).
- [17] Z.-X. Liu, Dissipative coupling induced UWB magnonic frequency comb generation, *Appl. Phys. Lett.* **124**, 032403 (2024).
- [18] X. Liang, Y. Cao, P. Yan, and Y. Zhou, Asymmetric magnon frequency comb, *Nano Lett.* **24**, 6730 (2024).
- [19] C. L. Ordóñez-Romero, B. A. Kalinikos, P. Krivosik, W. Tong, P. Kabos, and C. E. Patton, Three-magnon splitting and confluence processes for spin-wave excitations in yttrium iron garnet films: Wave vector selective Brillouin light scattering measurements and analysis, *Phys. Rev. B* **79**, 144428 (2009).
- [20] Z. Wang, H. Yuan, Y. Cao, and P. Yan, Twisted magnon frequency comb and Penrose superradiance, *Phys. Rev. Lett.* **129**, 107203 (2022).
- [21] B. Zhang, Z. Wang, Y. Cao, P. Yan, and X. Wang, Eavesdropping on spin waves inside the domain-wall nanochannel via three-magnon processes, *Phys. Rev. B* **97**, 094421 (2018).
- [22] Z. Zhou, X. Wang, Y. Nie, Q. Xia, and G. Guo, Spin wave frequency comb generated through interaction between propagating spin wave and oscillating domain wall, *J. Magn. Magn. Mater.* **534**, 168046 (2021).
- [23] N. Nagaosa and Y. Tokura, Topological properties and dynamics of magnetic skyrmions, *Nat. Nanotech.* **8**, 899 (2013).
- [24] A. Fert, N. Reyren, and V. Cros, Magnetic skyrmions: advances in physics and potential applications, *Nat. Rev. Mater.* **2**, 1 (2017).
- [25] A. Einstein, B. Podolsky, and N. Rosen, Can quantummechanical description of physical reality be considered complete?, *Phys. Rev.* **47**, 777 (1935).
- [26] E. Schrödinger, Discussion of probability relations between separated systems, in *Mathematical Proceedings of the Cambridge Philosophical Society*, Vol. 31 (Cambridge University Press, 1935) pp. 555–563.
- [27] R. Uola, A. C. Costa, H. C. Nguyen, and O. Gühne, *Quantum steering*, *Rev. Mod. Phys.* **92**, 015001 (2020).
- [28] V. Händchen, T. Eberle, S. Steinlechner, A. Sambrowski, T. Franz, R. F. Werner, and R. Schnabel, Observation of one-way Einstein-Podolsky-Rosen steering, *Nat. Photon.* **6**, 596 (2012).
- [29] Q. He, Q. Gong, and M. Reid, Classifying directional gaussian entanglement, Einstein-Podolsky-Rosen steering, and discord, *Phys. Rev. Lett.* **114**, 060402 (2015).
- [30] L. S. Madsen, F. Laudenbach, M. F. Askarani, F. Rortais, T. Vincent, J. F. Bulmer, F. M. Miatto, L. Neuhaus, L. G. Helt, M. J. Collins, et al., Quantum computational advantage with a programmable photonic processor, *Nature* **606**, 75 (2022).
- [31] J. Yin, Y. Li, S. Liao, M. Yang, Y. Cao, L. Zhang, J. Ren, W. Cai, W. Liu, S. Li, et al., Entanglement-based secure quantum cryptography over 1,120 kilometres, *Nature* **582**, 501 (2020).
- [32] B. K. Malia, Y. Wu, J. Martínez-Rincón, and M. A. Kasevich, Distributed quantum sensing with mode-entangled spin-squeezed atomic states, *Nature* **612**, 661 (2022).
- [33] J. Ren, P. Xu, H. Yong, L. Zhang, S. Liao, J. Yin, W. Liu, W. Cai, M. Yang, L. Li, et al., Ground-to-satellite quantum teleportation, *Nature* **549**, 70 (2017).
- [34] S. Liao, W. Cai, W. Liu, L. Zhang, Y. Li, J. Ren, J. Yin, Q. Shen, Y. Cao, Z. Li, et al., Satellite-to-ground quantum key distribution, *Nature* **549**, 43 (2017).
- [35] W. Zhang, T. van Leent, K. Redeker, R. Garthoff, R. Schwonek, F. Fertig, S. Eppelt, W. Rosenfeld, V. Scarani, C. C. Lim, et al., A device-independent quantum key distribution system for distant users, *Nature* **607**, 687 (2022).
- [36] J. Li, S.-Y. Zhu, and G. Agarwal, Magnon-photon-phonon entanglement in cavity magnomechanics, *Phys. Rev. Lett.* **121**, 203601 (2018).
- [37] Z. Zhang, M. O. Scully, and G. S. Agarwal, Quantum entanglement between two magnon modes via Kerr nonlinearity driven far from equilibrium, *Phys. Rev. Res.* **1**, 023021 (2019).
- [38] H. Tan, Genuine photon-magnon-phonon Einstein-Podolsky-Rosen steerable nonlocality in a continuously-monitored cavity magnomechanical system, *Phys. Rev. Res.* **1**, 033161 (2019).
- [39] D. Lachance-Quirion, S. P. Wolski, Y. Tabuchi, S. Kono, K. Usami, and Y. Nakamura, Entanglement-based single-shot detection of a single magnon with a superconducting qubit, *Science* **367**, 425 (2020).
- [40] H. Yuan, P. Yan, S. Zheng, Q. He, K. Xia, and M.-H. Yung, Steady bell state generation via magnon-photon coupling, *Phys. Rev. Lett.* **124**, 053602 (2020).
- [41] H. Yuan, Y. Cao, A. Kamra, R. A. Duine, and P. Yan, Quantum magnonics: When magnon spintronics meets quantum information science, *Phys. Rep.* **965**, 1 (2022).
- [42] X.-L. Hei, P.-B. Li, X.-F. Pan, and F. Nori, Enhanced tripartite interactions in spin-magnon-mechanical hybrid systems, *Phys. Rev. Lett.* **130**, 073602 (2023).
- [43] W. Zhong, Q. Zheng, G. Cheng, and A. Chen, Nonreciprocal genuine steering of three macroscopic samples in a spinning microwave magnon system, *Appl. Phys. Lett.* **123**, 134003 (2023).
- [44] S. Zheng, Z. Wang, Y. Wang, F. Sun, Q. He, P. Yan, and H. Y. Yuan, Tutorial: Nonlinear magnonics, *J. Appl. Phys.* **134**, 151101 (2023).
- [45] T. Qu, A. Hamill, R. H. Victora, and P. A. Crowell, Oscillations and confluence in three-magnon scattering of ferromagnetic resonance, *Phys. Rev. B* **107**, L060401 (2023).
- [46] F. Garcia-Sanchez, P. Borys, R. Soucaille, J.-P. Adam, R. L. Stamps, and J.-V. Kim, Narrow magnonic waveguides based on domain walls, *Phys. Rev. Lett.* **114**, 247206 (2015).
- [47] E. X. DeJesus and C. Kaufman, Routh-hurwitz criterion in the examination of eigenvalues of a system of nonlinear ordinary differential equations, *Phys. Rev. A* **35**, 5288 (1987).
- [48] D. Vitali, S. Gigan, A. Ferreira, H. Böhm, P. Tombesi, A. Guerreiro, V. Vedral, J. A. Zeilinger, and M. Aspelmeyer, Optomechanical entanglement between a movable mirror and a cavity field, *Phys. Rev. Lett.* **98**, 030405 (2007).
- [49] R. Simon, N. Mukunda, and B. Dutta, Quantum-noise matrix for multimode systems: U(n) invariance, squeezing, and normal forms, *Phys. Rev. A* **49**, 1567 (1994).
- [50] C. Weedbrook, S. Pirandola, R. García-Patrón, N. J. Cerf, T. C. Ralph, J. H. Shapiro, and S. Lloyd, Gaussian quantum information, *Rev. Mod. Phys.* **84**, 621 (2012).
- [51] G. Adesso, A. Serafini, and F. Illuminati, Extremal entanglement and mixedness in continuous variable systems, *Phys. Rev. A* **70**, 022318 (2004).
- [52] R. Simon, Peres-horodecki separability criterion for continuous variable systems, *Phys. Rev. Lett.* **84**, 2726 (2000).
- [53] I. Kogias, A. R. Lee, S. Ragy, and G. Adesso, Quantification of gaussian quantum steering, *Phys. Rev. Lett.* **114**, 060403 (2015).
- [54] Y.-D. Wang and A. A. Clerk, Reservoir-engineered entanglement in optomechanical systems, *Phys. Rev. Lett.* **110**, 253601 (2013).
- [55] C.-G. Liao, R.-X. Chen, H. Xie, and X.-M. Lin, Reservoir-engineered entanglement in a hybrid modulated three-mode optomechanical system, *Phys. Rev. A* **97**, 042314 (2018).

- [56] Q. Guo, M.-R. Wei, C.-H. Bai, Y. Zhang, G. Li, and T. Zhang, Manipulation and enhancement of einstein-podolskyrosen steering between two mechanical modes generated by two bogoliubov dissipation pathways, *Phys. Rev. Res.* **5**, 013073 (2023).
- [57] J. Xie, H. Yuan, S. Ma, S. Gao, F. Li, and R. A. Duine, Stationary quantum entanglement and steering between two distant macromagnets, *Quantum Sci. Technol.* **8**, 035022 (2023).
- [58] Z.-Q. Liu, Y. Liu, L. Tan, and W.-M. Liu, Reservoir engineering strong magnomechanical entanglement via dual-mode cooling, *Annalen der Physik* **535**, 2200660 (2023).
- [59] X. Shang, D.-D. Chen, H. Xie, G.-W. Lin, and X.-M. Lin, Generation of microwave-optics entanglement via reservoir engineering in cavity magnonic systems, *Phys. Lett. A* **493**, 129263 (2024).
- [60] S. L. Braunstein and P. Van Loock, Quantum information with continuous variables, *Rev. Mod. Phys.* **77**, 513 (2005).
- [61] V. Giovannetti, S. Lloyd, and L. Maccone, Quantum-enhanced measurements: beating the standard quantum limit, *Science* **306**, 1330 (2004).
- [62] Y. Cai, J. Roslund, V. Thiel, C. Fabre, and N. Treps, Quantum enhanced measurement of an optical frequency comb, *npj Quantum Inf.* **7**, 82 (2021).
- [63] C. Ockeloen-Korppi, E. Damskkägg, J.-M. Pirkkalainen, M. Asjad, A. Clerk, F. Massel, M. Woolley, and M. Sillanpää, Stabilized entanglement of massive mechanical oscillators, *Nature* **556**, 478 (2018).
- [64] S. Kotler, G. A. Peterson, E. Shojaei, F. Lecocq, K. Cicak, A. Kwiatkowski, S. Geller, S. Glancy, E. Knill, R. W. Simmonds, et al., Direct observation of deterministic macroscopic entanglement, *Science* **372**, 622 (2021).
- [65] C. W. Gardiner and M. J. Collett, Input and output in damped quantum systems: Quantum stochastic differential equations and the master equation, *Phys. Rev. A* **31**, 3761 (1985).